



Research on water retention and microstructure characteristics of compacted GMZ bentonite under free swelling conditions

Jiang-Feng Liu^{1,2} · Hong-Yang Ni¹ · Yong-Gui Chen² · Yu Wu¹ · Shuai-Bing Song¹ · Xu-Lou Cao¹ · Wen-Bo Bao¹ · Hai Pu¹ · Xian-Biao Mao¹

Received: 12 April 2018 / Accepted: 13 August 2018 / Published online: 21 August 2018
© Springer-Verlag GmbH Germany, part of Springer Nature 2018

Abstract

In this study, water retention tests under free swelling conditions were performed to investigate the water intake (or loss) behaviour of compacted GMZ bentonite. First, the water retention characteristics were investigated, and then the microscopic pore structure was observed by environmental scanning electron microscope (ESEM). The results indicate that GMZ bentonite has a strong swelling (or a limited shrinkage ability) due to water intake (loss). The suction behaviour of GMZ bentonite is similar to MX80 bentonite and FEBEX bentonite. We also find that the confinement conditions can affect the suction behaviour of the material, especially at high relative humidity (RH). Additionally, a mathematic model can fit the mass change data very well. Microscopic tests show that the granular sensation of GMZ bentonite is obvious for a sample at low RH. With the increase in RH, the surface of GMZ bentonite becomes more smooth. The differences in the porosities calculated by the macroscopic and microscopic tests can be attributed to image resolution. The inter-laminar pores and intra-aggregate pores cannot be observed by the ESEM method. In addition, ESEM observation can provide an intuitive basis for the further research of the seepage property of GMZ bentonite.

Keywords GMZ bentonite · High-level radioactive waste · Free swelling conditions · Water intake (loss) · Microscopic observation

Introduction

With the rapid development of the national economy, energy shortages have gradually become a serious problem in many countries, including China. The Chinese government has paid an increasing attention to the utilization and development of nuclear energy. The development of nuclear energy has produced a great deal of nuclear waste, and how to properly and safely dispose of this nuclear waste, especially the

high-level radioactive waste, has become an urgent problem. For the final disposal of high-level radioactive waste, the feasibility of the scheme accepted by many countries is the deep geological disposal of high-level radioactive waste (Chen et al. 2014; Cui et al. 2012; Liu et al. 2014a, b; Ye et al. 2014a). After curing and filling, the waste is buried in a stable stratum at a depth of 300–500 m underground and is isolated from the human environment.

The design concept of a “multi barrier system” is adopted in deep geological disposal, including geological barriers of surrounding rock, engineering barriers based on buffer / backfill material and waste storage vessels (Alonso et al. 2005; Komine 2004; Liu et al. 2014a). In this context, bentonite or bentonite-based materials are chosen by many countries as buffer or backfill materials. In particular, the initial state of bentonite is only partially saturated. With time, the swelling of bentonite will occur due to water absorption from the surrounding host rock, closing up any construction gaps in the repository, and hence sealing is obtained (Horseman et al. 1999; Villar and Lloret 2007; Wang et al. 2012). These gaps are widely distributed between the bentonite

✉ Jiang-Feng Liu
jeaffliu@hotmail.com

✉ Yong-Gui Chen
cyg@tongji.edu.cn

¹ The State Key Laboratory for GeoMechanics and Deep Underground Engineering, and School of Mechanics and Civil Engineering, China University of Mining and Technology, Xuzhou 221116, China

² Key Laboratory of Geotechnical and Underground Engineering of Ministry of Education, Tongji University, Shanghai, China

blocks themselves, canister and blocks, blocks and host rock and the fractures in the EDZ (excavation damage zone) of the host rock due to construction. Regarding the confinement conditions, the bentonite materials first experience free swelling (prior to filling the gaps) before being confined by the host rock. During this period, the pore structure changes gradually due to the swelling of the bentonite, which can further affect its hydraulic property. Therefore, a proper understanding of the water retention and micro-pore structure behaviour of the compacted bentonite or bentonite-based material during the hydration process is critical for the evaluation of its sealing behaviour.

The water retention property of compacted bentonite when in contact with water has been widely investigated by many researchers. The initial physical properties (dry density, water content, and clay mineral content) and the initial state (loose or compacted) can largely affect the water retention property of compacted bentonite (Komine and Ogata 1994, 1999; Lloret and Villar 2007; Marcial et al. 2002; Villar and Lloret 2008; Wang et al. 2012). In addition, the effect of temperature and the chemical composition of the saturated fluid also have an influence on the water retention property of compacted bentonite (Shirazi 2010; Ye et al. 2013, 2014b). The water retention property of compacted bentonite also has a close relationship with its hydraulic behaviour, which is a key indicator to evaluate the sealing ability of the bentonite buffer (Camillis et al. 2016; Chen et al. 2015; Komine 2010; Mishra et al. 2011). Wetting leads to the increase in water content, and hence the hydraulic conductivity decreases, whereas wetting also leads to the swelling of bentonite, and hence increases its porosity and the hydraulic conductivity (Liu et al. 2015). This means the increase in water content and the porosity caused by wetting play a contrary effect in the change of the hydraulic behaviour of compacted bentonite. Although many researchers have made significant contribution in this field, there is still some work that should be done to clarify its swelling (or shrinkage) mechanism, especially at the microscopic level. In recent decades, some researchers have investigated the microscopic pore structure of porous media by means of

SEM, NMR, CT and FIB/SEM (Blunt et al. 2013; Houben et al. 2013; Li et al. 2018; Song et al. 2015). Within these methods, SEM is the most widely applied because of its high resolutions and low cost. In addition, SEM images can supply direct information on the real pore network and can qualitatively and quantitatively characterize the pore structures of the porous media.

This study focuses on the water properties of the GMZ bentonite under free swelling conditions and different relative humidity (RH). A mathematic model is chosen to simulate the mass variation under different RH. Then, a SFG model is utilized to predict the change in the porosity of compacted GMZ bentonite under different RH. Lastly, we further analyse its swelling (shrinkage) property from the microscopic level by the method of ESEM.

Experimental methods

Materials and sample preparation

The material used in this study is GMZ bentonite that obtained from the northern Chinese Inner Mongolia autonomous region, 300 km northwest of Beijing. The main mineral compositions of GMZ bentonite are listed in Table 1. It can be seen that the main mineral of the GMZ bentonite is clay mineral, whereas montmorillonite occupies 98% of total clay minerals. The particle-size distribution of GMZ bentonite powder measured with the laser scattering method is shown in Fig. 1a.

These powders were pre-conditioned in a desiccator with an RH of 43% and a temperature of 22 °C until a constant mass ($w = 10.20\% \pm 0.10$) was obtained. This period usually last more than 1 month to obtain the mass stabilization. According to the water content and target dry density ($\rho_d = 1.70 \text{ g/cm}^3 \pm 0.05$) and dimension of the sample [20 (height) × 25 mm (diameter)], we can calculate the mass of the powder that needs to compact the sample. It should be noted that the dry density was calculated with the initial volume, i.e., the sample just after compaction. Then, the

Table 1 Mineral species and content of GMZ bentonite powder

Mineral species and content (%)						Content of clay mineral (%)	
Quartz	Potash feldspar	Plagioclase	Calcite	Christobalite	Clinoptilolite		
23	1.5	4.5	/	8	4.7	58.3	
Relative content of clay minerals (%)						Mixed-layer ratio M, %	
M	I/M	I	K	C	C/M	I/M	C/M
98	/	2	/	/	/	/	/

M is montmorillonite, I is illite, K is kaolinite, C is chlorite

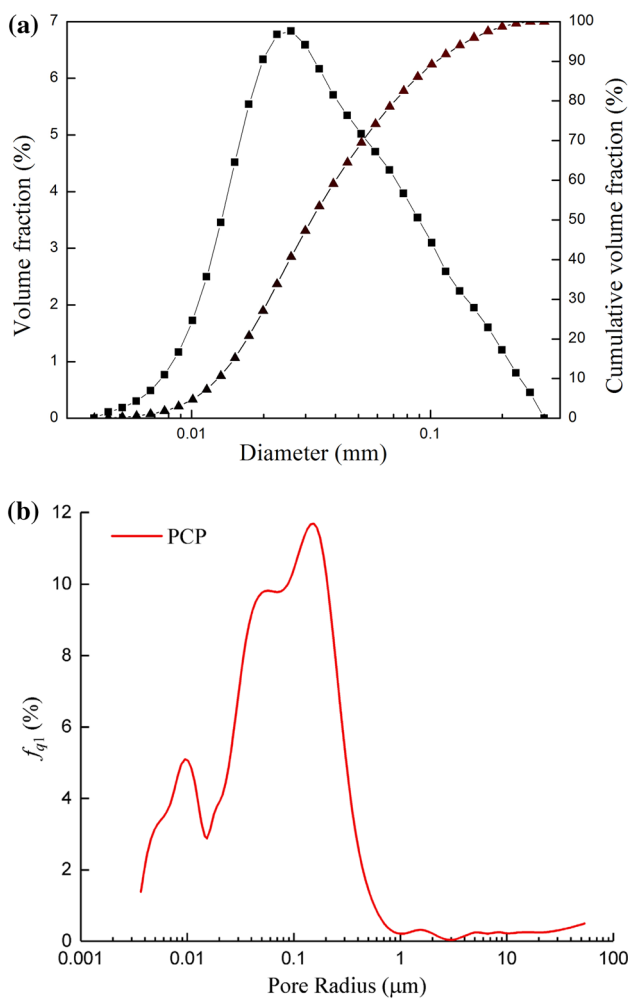


Fig. 1 **a** Particle-size distributions of GMZ bentonite powder, **b** pore-size distribution of GMZ bentonite

prepared powders were compacted in a dedicated steel cylindrical mould with a compression speed of 0.1 mm/min. The first sample was put in a drying oven with a temperature of 105 °C to check the water content and dry density. If the target values were reached, the other samples were prepared. The obtained physical characteristics for all samples are given in Table 2.

Table 2 Primary characteristic of GMZ bentonite sample

	GM00	GM01	GM02	GM03	GM04	GM05
m_{ini} (g)	18.30	18.37	18.28	18.31	18.39	18.37
d (mm)	25.22	25.25	25.25	25.24	25.23	25.23
h (mm)	20.01	19.96	20.01	20.00	20.05	20.04
m_{dry} (g)	17.02	–	–	–	–	–
ρ_d (g/cm ³)	1.70	–	–	–	–	–

m_{ini} is the mass of the sample just after compaction; d and h are the diameter and height of the sample; m_{dry} is the mass of the sample after oven-drying; ρ_d is dry density of the sample. For samples GM01 ~ GM05, dry density cannot be measured because they were cut into small pieces to perform SEM test after water retention test

In this study, pressure-controlled porosimetry (PCP) was used to investigate the pore size distribution (PSD) of the GMZ sample. As shown in Fig. 1 (b), the pore size of compacted GMZ bentonite exists mainly within the range of 0.01–1.0 μm.

Experimental procedure

Both cylindrical samples and small cubic pieces (used for ESEM testing) were placed in the desiccators with different RH, including 11%, 75%, 85%, 95% and 98%. These relative humidities were provided by various salt solutions, see Table 3. These desiccators were put in a room with a temperature of 22°C±1 °C. Mass and dimension (just for cylindrical samples) were regularly measured and recorded every 0.5 h, 1 h, 2 h, 4 h, 8 h, and followed by once per week. The dimensions were measured regularly during these steps using digital calipers that are accurate to within 0.01 mm. Recording was stopped when the mass variation came within 0.01 g in three consecutive measurements.

ESEM was chosen to observe the pore structure of the GMZ bentonite under different RH. Compared with the traditional SEM method, ESEM can prevent water loss during the observation. The entire experimental procedure is shown in Fig. 2.

Table 3 Salt solutions and corresponding RHs

RH	11%	75%	85%	95%	98%
Salt solution	LiCl	NaCl	KCl	KNO ₃	K ₂ SO ₄

Fig. 2 Experimental procedure

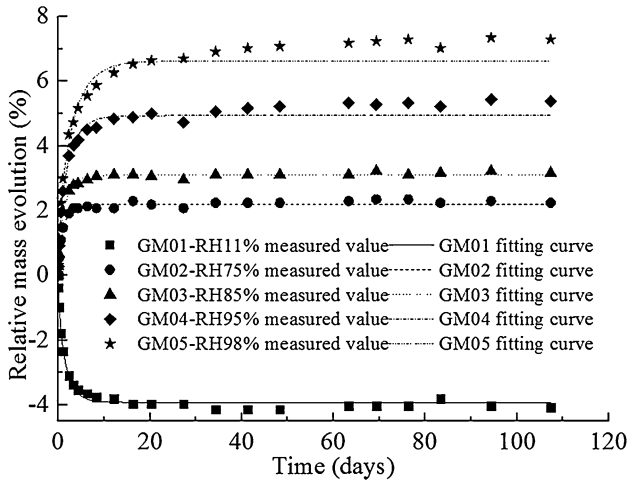
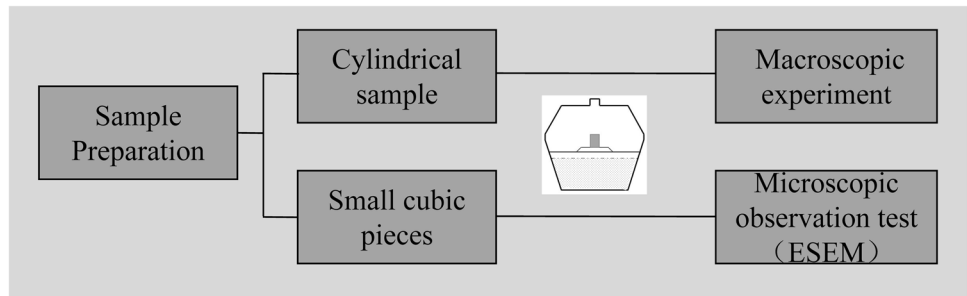


Fig. 3 Evolution of relative mass vs. time: measured data and fitting result

Results and analysis

Water retention characteristics

Mass evolution under different RH

Figure 3 shows the relative mass variation vs. time of GMZ samples under different RH. It can be found that the samples absorb water under RH=75%, 85%, 95%, and 98%, whereas the sample loses water under RH=11%. For all samples, mass increase (loss) mainly occurred during the first week, more than 90% of the total mass increase (or loss). There is not much difference regarding the time needed for the mass of the sample to become stable. Overall, mass variation becomes stable after 1 month.

The sorption of the spherical sample under constant RH can be modelled by a series of exponential functions (Crank 1975),

$$M_t = M_f \left[1 - \frac{6}{\pi^2} \sum_1^{\infty} \frac{1}{n^2} \exp \left(-\frac{D\pi^2}{R_s^2} n^2 t \right) \right], \quad (1)$$

Table 4 Fitting parameters

RH	m_f	c	R^2
11%	-3.92	0.5209	0.955
75%	2.2	0.6894	0.9866
85%	3.1	0.5866	0.9941
95%	4.94	0.3955	0.9785
98%	6.62	0.2788	0.9711

where M_t is the total mass passed from the surface of a sphere in a finite time, M_f is the total mass passed after the infinitely long time, D is the diffusion coefficient and R_s is the radius of the sphere.

Tada and Watanabe (2005) rewrite the above equation as

$$M_t = M_f \left(1 - b \sum_1^N \frac{1}{n^2} \exp(-cn^2t) \right), \quad (2)$$

where b is the inverse of the sum of $\sum_1^N 1/n^2$ and c is equal to $D\pi^2/R_s^2$.

Tada and Watanabe (2005) found that Eq. (2) ($N=5$ is enough) can simulate the sorption process of the porous material even though the sample is not strictly spherical. Similarly, Liu (2011) also verified that this conclusion is feasible for cylindrical samples. Therefore, we attempted to simulate the experimental results of sorption with Eq. (2). As shown in Fig. 3 and Table 4, the mathematic model can simulate the experimental results very well, especially at the initial phase of the sorption.

It is assumed that the equivalent radius R of the samples is constant, because the sample sizes in our tests are invariable. The parameter c is equal to $D\pi^2/R_s^2$ in Eq. 2. Then, we can deem that the parameter c is proportional to the diffusion coefficient D and the variation in the value of the parameter c directly reflects the variation in the diffusion coefficient D . Thus, for the GMZ bentonite, c varies from 0.2788 to 0.6894 and this indicates that RH deviation has a certain influence on the diffusion coefficient. For GMZ bentonite, parameter c generally decreases when the RH increases in the sorption process (in the case of RH=78%~98%), and therefore it can be said that D increases when RH decreases.

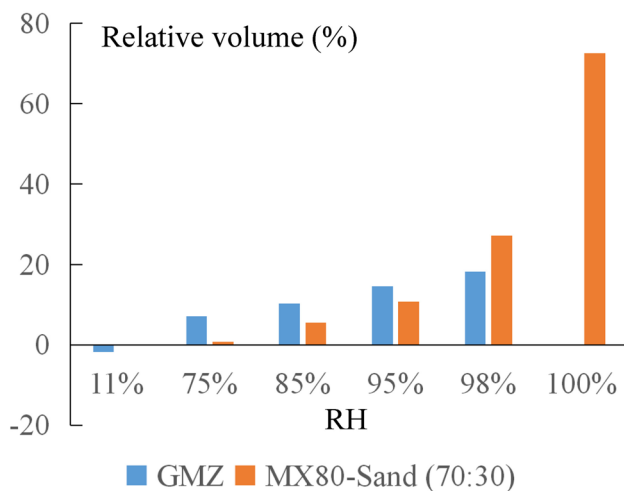


Fig. 4 Comparison of relative volume variation under different RHs between GMZ bentonite and MX80 bentonite–sand mixture

Volume evolution under different RH

Figure 4 presents the relative volume variation vs. time of GMZ samples under different RH. The overall trend is similar to the relative mass variation. It is amazing that the volume increase at RH = 98% is 18.28%. At RH = 100%, we did not measure the volume change of GMZ bentonite due to some reasons. According to our previous research, the volume change is 72.48% for MX80 bentonite–sand mixture ($\rho_d = 1.7 \text{ g/cm}^3$) at RH = 100% (see Fig. 4). Therefore, it is foreseen that the volume change of GMZ bentonite in RH = 100% is also very high, which hints a strong swelling ability of GMZ bentonite. As a result, the bentonite can fill the technical voids (e.g., the voids between the canister and the buffer and between the host rock and the buffer) in situ when contacting with water from the host rock, which is favourable for the sealing of the bentonite buffer.

At RH = 11%, the relative volume decreases by 1.85%, which indicates a limited shrinkage ability of GMZ bentonite when losing water. A similar phenomenon was also observed by Liu et al. (2014b) for MX80 bentonite–sand mixture under free swelling conditions, see Fig. 4. It is found that GMZ bentonite has a higher swelling ability than MX80-sand mixture at RH = 75%~95% except at RH = 98%. In fact, the swelling ability is strongly dependent on the composition (e.g., montmorillonite content) and the initial state of the compacted materials (e.g., dry density and water content). Regarding the two materials, they have the same initial dry density (1.7 g/cm^3) and different initial water (10.28 vs. 15.2%) content and compositions. Anyhow, both of the two materials show significant swelling ability when the materials approach saturation under free-swelling conditions.

WRCs of GMZ bentonite

Figure 5 presents the wetting path of the water retention curves (WRCs) for GMZ bentonite obtained under free swelling conditions (unconfined). It is found that the wetting path is nonlinear. Compared with other two kinds of bentonite (MX80 bentonite and FEBEX bentonite), their suction behaviours are very close, especially at high suction. It seems that the water retention ability of MX80 bentonite is higher than the other two kinds of bentonite at the low suction. However, the disparity is limited. The limited difference is related to their small differences in the mineral compositions.

Regarding the confinement conditions, the effect is not clear at low water content (high suction), whereas an obvious difference is observed at high water content (low suction). As indicated by many researchers (Cariou et al. 2013; Hoffmann et al. 2007; Liu et al. 2018), bentonite is a double-porosity network material. At high suction (low RH), there is sufficient space at an inter-aggregate scale to allow the swelling of intra-aggregate pores. As a result, the water retention behaviour is insensitive to the confinement conditions before the inter-aggregate pores are completely filled with swelling clay aggregate. At low suction (high RH), the volume of inter-aggregate pores will increase because of the swelling of the intra-aggregate pores. As a result, there is an increase in the total volume and more water is absorbed when the swelling condition is unconfined. However, this is not the case in a confined condition.

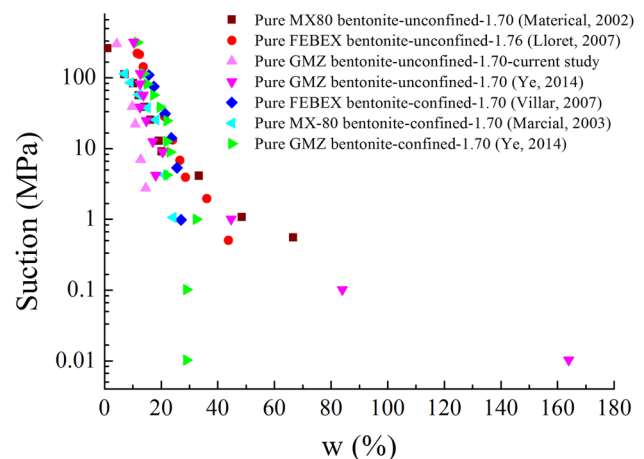


Fig. 5 Water retention curves of GMZ bentonite, MX80 bentonite and FEBEX bentonite

Void ratio evolution

Evolution of void ratio under different RH

Void ratio is an important factor to evaluate the hydraulic property of the unsaturated soil. The initial void ratio is given by

$$e_{ini} = \frac{V_{v-ini}}{V_s} = \frac{V_{ini} - V_s}{V_s}, \tag{3}$$

where e is the void ratio, V_{ini} is the initial volume of the sample, V_{v-ini} is the initial volume of the voids and V_s is the volume of the solid particle. In addition, V_s can be calculated by the following equation:

$$V_s = \frac{m_s}{\rho_s}, \tag{4}$$

where m_s is solid particle mass, which is equal to the dry mass $m_d \cdot \rho_s$ is the granule density, which is 2.64 g/cm³ for GMZ bentonite. Therefore, we can rewrite Eq. (3) as

$$e_{ini} = \frac{V_{ini} - V_s}{V_s} = \frac{V_{ini}}{m_s} \rho_s - 1, \tag{5}$$

During the sorption (or desorption) process, the void ratio e_t at time t can be calculated as follows:

$$e_t = \frac{V_{v-t}}{V_s} = \frac{(V_t - V_s)\rho_s}{m_s} = \frac{(V_t - \frac{m_s}{\rho_s})\rho_s}{m_s} = \frac{V_t\rho_s - m_s}{m_s} = \frac{V_t\rho_s}{m_d} - 1, \tag{6}$$

where V_t is the volume of the sample at time t which can be measured directly. As shown in Fig. 6, the void ratio increases rapidly during the first week, and then its value tend to be stable. Again, it is found that GMZ bentonite has a strong swelling (a limited shrinkage) ability at high

(low) RH. The changes in the void ratio are 0.028, 0.109, 0.158, 0.226, 0.283 and 0.312 for RH = 11%, 75%, 85%, 95% and 98%. The difference of the void ratio at RH = 11% and RH = 98% is 0.312, which hints at an apparent change in the pore structure under high RH (low suction). This phenomenon will be further analysed with ESEM technology.

Relationship between void ratio and suction

For unsaturated soil, the volume change is due to the suction change and (or) the action of external stress. Sheng et al. (2008) proposed a SFG model, which can simulate the deformation of the unsaturated soil.

$$d\varepsilon_V = -\frac{dv}{v} = \lambda_{vp} \frac{d\bar{p}}{(\bar{p} + s)} + \lambda_{vs} \frac{ds}{(\bar{p} + s)}, \tag{7}$$

where ε_V is the volume change, $v = 1 + e$ is the specific volume and e is the void ratio, $\bar{p} = p - u_a$ is the mean net stress, u_a is the pore-air pressure, $s = u_a - u_w$ is the suction, λ_{vp} is the normally consolidated consolidation coefficient, λ_{vs} is the consolidation coefficient corresponding to the suction and λ_{vs} gradually decreases to zero at high soil suctions. Usually, λ_{vs} can be taken from

$$\lambda_{vs} = \begin{cases} \lambda_{vp} & s < s_{sa} \\ \lambda_{vp} \frac{s_{sa} + 1}{s + 1}, & s \geq s_{sa} \end{cases}, \tag{8}$$

where s_{sa} is the saturation suction; 1 is added to avoid the singularity of functions and can be overlooked if s_{sa} is not equal to zero. According to experimental data, the suction-void ratio curve can be fitted very well where $\lambda_{vp} = 0.049$, see Fig. 7. According to this model (curve), it is easy to predict the void ratio (porosity) at a given suction (RH).

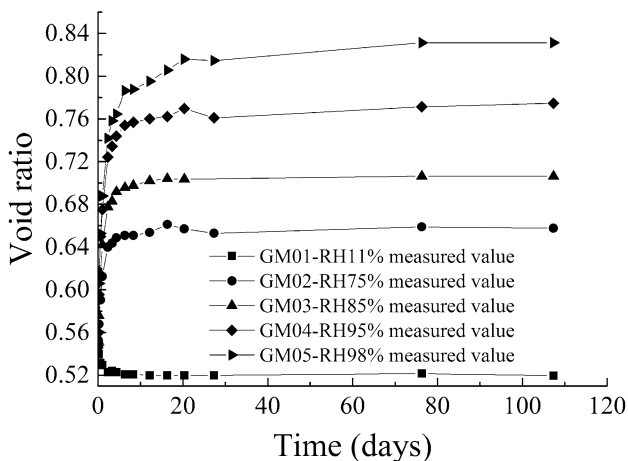


Fig. 6 Evolution of void ratio with time

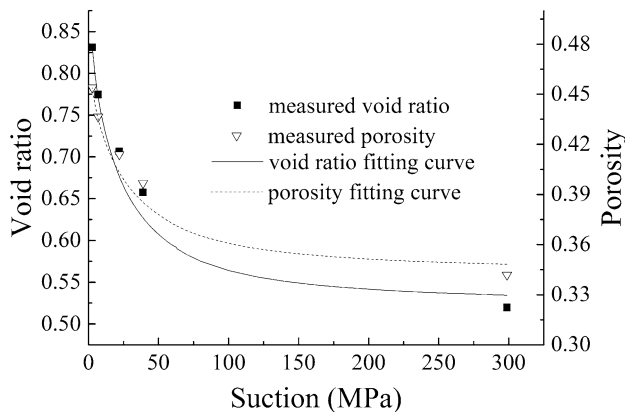


Fig. 7 Relationship between the void ratio and suction

Micro-analysis of GMZ bentonite

Evolution of the microstructure of GMZ bentonite under different RH

As indicated before, the ESEM method is chosen to analyse the changes in the pore structure of GMZ bentonite under different RH (suction). As shown in Fig. 8a–c, we chose the samples under RH = 11%, 75% and 85% of the three representative RHs to analyse. It is clear that the aggregates are densely assembled and there are many small and connected pores in the surface of the sample at low RH. With the increase in RH (or decrease in suction), the clay particles absorb water and fill some pores, which make the surface of the sample look smoother. The numbers of small and connected pores decrease greatly. Other researchers attribute this phenomenon to the exfoliation of the particle when RH increases (Wang et al. 2013). Considering the good swelling ability of GMZ bentonite (Fig. 4), the former explanation seems to be more suitable. It seems that the porosity decreases when RH increases, because the number of the pores decreases significantly (see Fig. 8 (c)). However, according to Fig. 7, the porosity increases with the increase in RH (decrease in suction). This difference will be analysed later.

Regarding the seepage property of GMZ bentonite, it seems to be that there are fewer pores (connected pores) in the surface of the sample at high RH, which makes fluid migration more difficult. However, the volume of the sample actually increases at high RH, which hints that there are more pores for fluid migration. There exists a contradiction between the observation from the ESEM image and the actual volume (or porosity) measured by the suction test. This contradiction is closely related to the pore structure of the bentonite.

Quantitative analysis of porosity (void ratio)

To quantify the change of the porosity, we use box counting method in the MATLAB to analyse the ESEM photograph and to determine the representative elementary area (REA). It should be clarified that the calculation only involve 2D image only, so it is not really the porosity. To make the analysis more statistically reliable, we select five different locations of the image (top left, top right, center, bottom left, bottom right) (see Fig. 9a). Then, a box is wrapped over the top of the image and is served as the virtual boundary of the image. The image is binarized using the determined threshold value. The criterion for the determination of the threshold value is based on the consideration of two factors. The first factor is the discrepancy between the thresholded and the original images, while the second factor is the number of bits required to represent the thresholded image. More

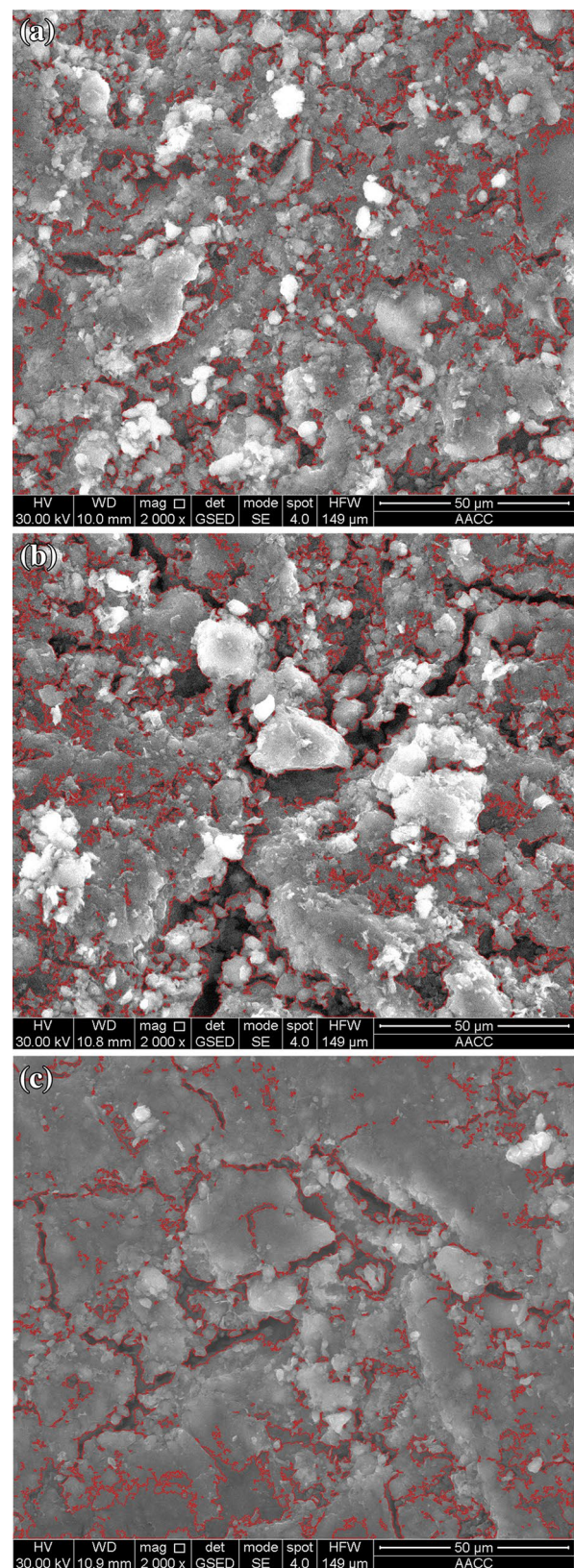


Fig. 8 ESEM photographs of GMZ bentonite samples equilibrated at **a** RH = 11%, **b** RH = 75% and **c** RH = 98%

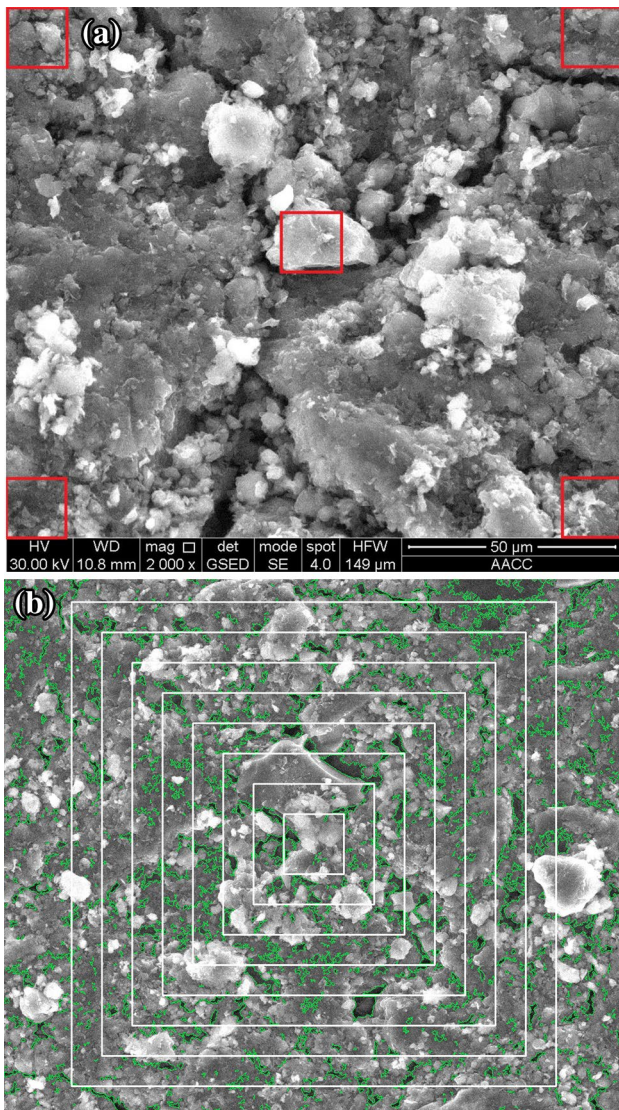


Fig. 9 **a** The different locations selected at ESEM image for the determination of REA, **b** Different size of REA

details can be found in Yen et al. (1995). The internal porosity in the virtual boundary is calculated by dividing the area of the pores in the virtual boundary the box by the area of the box. Lastly, the boundary is increased by every 50-pixel points until arriving at the margin of the image and the corresponding porosity is calculated (see Fig. 9b).

Figure 10a–c present the porosities calculated by analysing the ESEM images from RH = 11%, 75% and 98%. It is found that the values of the porosity fluctuate obviously when the box size is less than 30 μm. This means that this box size cannot represent macro GMZ bentonite sample due to the poor homogeneity. With the increase in the box size, the value of the porosity at the same position is gradually converged and the curve tends to be gentle. The convergence value is the porosity of the GMZ bentonite sample under

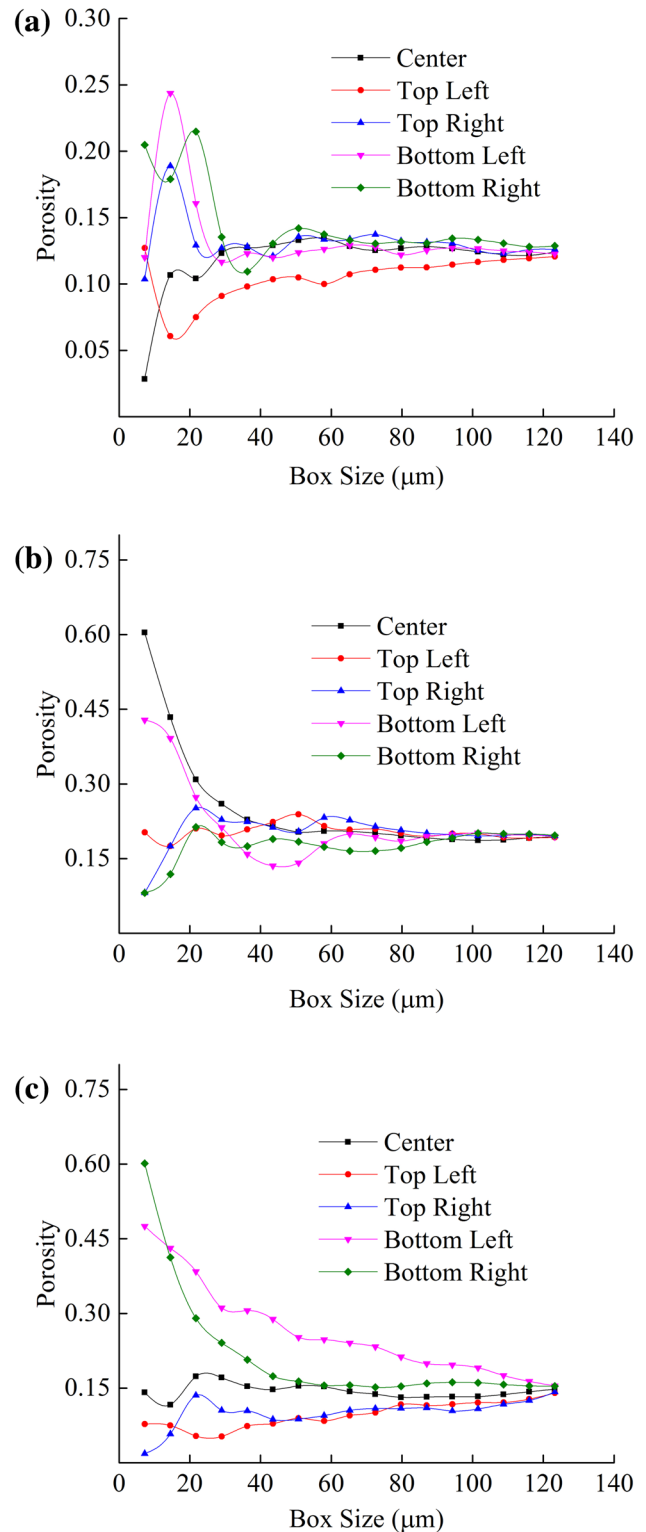


Fig. 10 Porosity variation as a function of box size: **a** RH = 11%, **b** RH = 75% and **c** RH = 98%

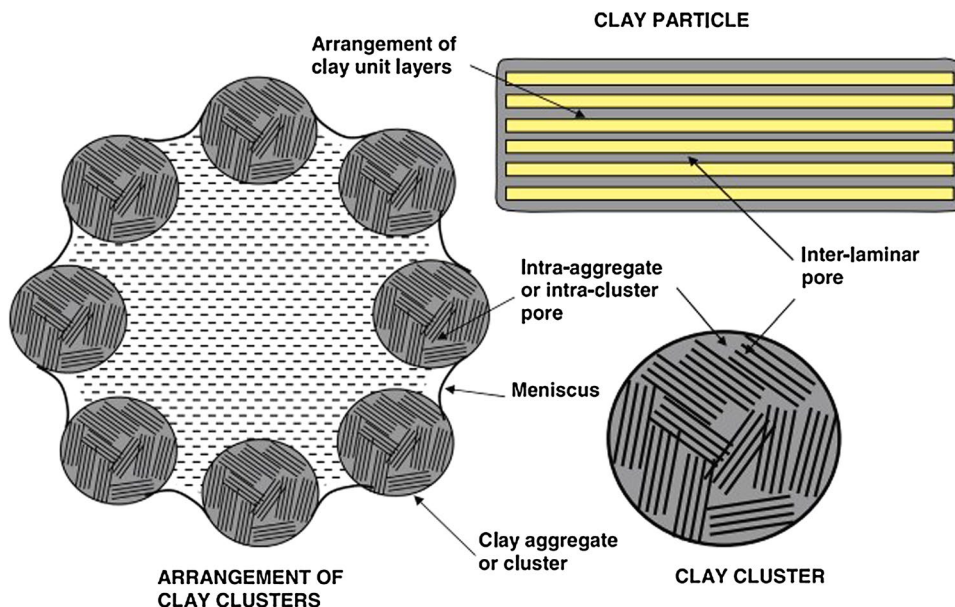
the corresponding RH. When the stable value is reached, the corresponding box size is the length of the characterization unit. These values are 100 μm for RH=11%, 90 μm for RH=75% and 110 μm for RH=98%, and the corresponding unit areas are 10000μm², 8100μm² and 12100μm², respectively.

Based on ESEM images, the calculated porosities (apparent porosity) are 0.13 (RH=11%), 0.19 (RH=75%) and 0.14 (RH=98%), which are largely different from the values calculated by the volume changes (macro-porosity) in the suction test (see Table 5). This difference is closely related to the pore structure of the bentonite and the threshold value chosen for the binarization of SEM image. As shown in Fig. 11, the basic unit of bentonite particles is a crystal layer. There are some small pores (Pore I: inter-laminar pore) in the crystal layer, and a number of crystal layers compose of a granule. These granules gather together to form aggregates, and there exist some pores in the aggregate (Pore II: intra-aggregate pore), and between the aggregates and aggregates (Pore II: inter-aggregate pore). That is, the pores in the bentonite are composed of these three kinds of pores. With the increase in RH, the clay particles absorb water and swell, leading to the increase in the porosity. However, with the ESEM images, only Pore III in the surface of the sample can be observed, and the porosity calculated with ESEM images is in fact the apparent porosity ϕ_a ,

Table 5 The porosity calculated with different methods

Porosity	RH=11%	RH=75%	RH=98%
Volume change method	0.34	0.40	0.45
ESEM method	0.13	0.19	0.14

Fig. 11 Schematic distributions of the basic unit of bentonite particles (Agus et al. 2010)



$$\phi_a = \frac{V_{III}}{V_I + V_{II} + V_{III} + V_S}, \tag{9}$$

where V_I is the volume of inter-laminar pore, V_{II} is the volume of intra-aggregate pore, V_{III} is the volume of inter-aggregate pore and V_S is the volume of solid particle (see Fig. 12). From RH=75% to RH=98%, V_{III} decreases while V_I and V_{II} increase, which lead to a decrease in ϕ_a . With the traditional method, the porosity calculated by the volume change is in fact the macro-porosity ϕ_m ,

$$\phi_m = \frac{V_I + V_{II} + V_{III}}{V_I + V_{II} + V_{III} + V_S}. \tag{10}$$

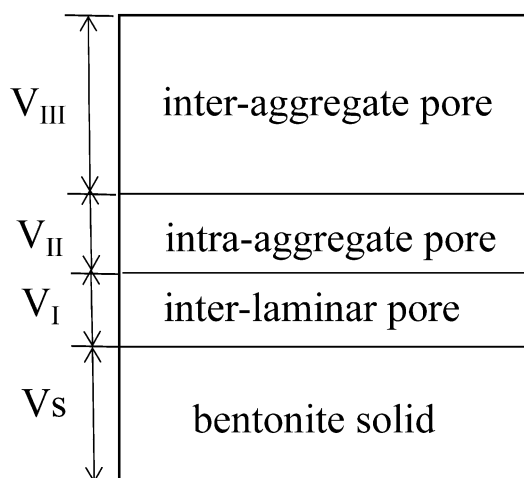


Fig. 12 Schematic diagram for the calculations of apparent porosity and macro-porosity

From the Eqs. (8) and (9), it is clear that why θ_a is currently smaller than θ_m . Generally, there are some empirical formulas, which can predict the fluid permeability from the porosity. However, the inter-laminar pores and intra-aggregate pores contribute little to the transport of fluid flow. It means that we should adopt θ_a rather than θ_m to calculate the permeability. Overall, the two-dimensional microscopic observation can be used to observe the evolution of pore structure more intuitively, which can be used to further study the seepage characteristics of GMZ bentonite and to provide some micro-scale basis.

Conclusion

The water retention and microstructure characteristics of compacted GMZ bentonite were investigated by both theoretical analysis and microscopic observation. It is found that GMZ bentonite has a good swelling ability at high RH and a limited shrinkage ability at low RH, which is favourable for the sealing of the entire artificial barrier. Compared with MX80 bentonite and FEBEX bentonite, their suction behaviours are very close, especially at high suction. Regarding the confinement conditions, their effects are obvious at low suction (high RH), whereas the effects can be overlooked at high suction (low RH).

The mathematic mode can fit the experimental data very well with a very high fitting coefficient. Mass evolution data indicate that RH has a certain effect on the diffusion coefficient, and its value increases with the decrease in the RH. With the SFG model, it is possible to predict the porosity (void ratio) when the sample reaches the stable state under a certain RH (or suction).

ESEM observation shows that there are many small and connected pores in the surface of the sample at low RH, and the granular sensation is obvious. With the increase in RH, the numbers of small pores and connected pores decrease greatly and the surface of the sample becomes smoother. The value of porosity calculated by the ESEM image is largely different from the value measured in the suction test. This phenomenon has a close relationship with the pore structure of GMZ bentonite, because the inter-laminar pores and intra-aggregate pores cannot be observed by ESEM technology. Additionally, ESEM observation can supply some intuitive basis for the further research of the seepage property of GMZ bentonite.

Acknowledgements The authors are grateful to the support of the Fundamental Research Funds for the Central Universities (China University of Mining and Technology) (2017QNA29).

References

- Agus SS, Schanz T, Fredlund DG (2010) Measurements of suction versus water content for bentonite-sand mixtures. *Can Geotech J* 47:583–594
- Alonso EE, Romero E, Hoffmann C, García-Escudero E (2005) Expansive bentonite–sand mixtures in cyclic controlled-suction drying and wetting. *Eng Geol* 81:213–226
- Blunt MJ, Bijeljic B, Hu D, Gharbi O, Iglauer S, Mostaghimi P, Paluszny A, Pentland C (2013) Pore-scale imaging and modeling. *Adv Water Resour* 51:197–216
- Camillis MD, Emidio GD, Bezuijen A, Verástegui-Flores RD (2016) Hydraulic conductivity and swelling ability of a polymer modified bentonite subjected to wet–dry cycles in seawater. *Geotext Geomembr* 44:739–747
- Cariou S, Dormieux L, Skoczylas F (2013) An original constitutive law for Callovo-Oxfordian argillite, a two-scale double-porosity material. *Appl Clay Sci* 81:18–30
- Chen L, Liu YM, Wang J, Cao SF, Xie JL, Ma LK, Zhao XG, Li YW, Liu J (2014) Investigation of the thermal-hydro-mechanical (THM) behavior of GMZ bentonite in the China-Mock-up test. *Eng Geol* 172:57–68
- Chen YG, Zhu CM, Ye WM, Cui YJ, Wang Q (2015) Swelling pressure and hydraulic conductivity of compacted GMZ01 bentonite under salinization–desalinization cycle conditions. *Appl Clay Sci* 114:454–460
- Crank J (1975) *The mathematics of diffusion*, 2nd ed. WSEAS TRANSACTIONS on SYSTEMS and CONTROL Ahmet Kuzu, Metin Gokasan, Seta Bogosyan ISSN: 1991-8763, Issue 8(3):625–626
- Cui S-L, Zhang H-Y, Zhang M (2012) Swelling characteristics of compacted GMZ bentonite–sand mixtures as a buffer/backfill material in China. *Eng Geol* 141–142:65–73
- Hoffmann C, Alonso EE, Romero E (2007) Hydro-mechanical behaviour of bentonite pellet mixtures. *Phys Chem Earth A/B/C* 32:832–849
- Horseman ST, Harrington JF, Sellin P (1999) Gas migration in clay barriers. *Eng Geol* 54:139–149
- Komine H (2004) Simplified evaluation for swelling characteristics of bentonites. *Eng Geol* 71:265–279
- Komine H (2010) Predicting hydraulic conductivity of sand-bentonite mixture backfill before and after swelling deformation for underground disposal of radioactive wastes. *Eng Geol* 114:123–134
- Komine H, Ogata N (1994) Experimental study on swelling characteristics of compacted bentonite. *Can Geotech J* 31:478–490
- Komine H, Ogata N (1999) Experimental study on swelling characteristics of sand-bentonite mixture for nuclear waste disposal. *Soils Foundations* 39:83–97
- Li X, Kang Y, Haghghi M (2018) Investigation of pore size distributions of coals with different structures by nuclear magnetic resonance (NMR) and mercury intrusion porosimetry (MIP). *Measurement* 116:122–128
- Liu J (2011) Etude expérimentale de la perméabilité relative des matériaux cimentaires et simulation numérique du transfert d'eau dans le béton. PhD thesis, Ecole Centrale De Lille
- Liu JF, Davy CA, Talandier J, Skoczylas F (2014a) Effect of gas pressure on the sealing efficiency of compacted bentonite–sand plugs. *J Contam Hydrol* 170:10–27
- Liu JF, Skoczylas F, Liu J (2014b) Experimental research on water retention and gas permeability of compacted bentonite/sand mixtures. *Soils Found* 54:1027–1038
- Liu JF, Skoczylas F, Talandier J (2015) Gas permeability of a compacted bentonite–sand mixture: coupled effects of water content, dry density, and confining pressure. *Can Geotech J* 52:1159–1167

- Liu JF, Wu Y, Cai CZ, Ni HY, Cao XL, Pu H, Song SB, Pu SY, Skoczylas F (2018) Investigation into water retention and gas permeability of Opalinus clay. *Environ Earth Sci* 77:213
- Lloret A, Villar MV (2007) Advances on the knowledge of the thermo-hydro-mechanical behaviour of heavily compacted “FEBEX” bentonite. *Phys Chem Earth A/B/C* 32:701–715
- Marcial D, Delage P, Yu JC (2002) On the high stress compression of bentonites. *Can Geotech J* 39:812–820
- Houben ME, Desbois G, Urai JL (2013) Pore morphology and distribution in the Shaly facies of Opalinus Clay (Mont Terri, Switzerland): insights from representative 2D BIB–SEM investigations on mm to nm scale. *Appl Clay Sci* 71:82–97
- Mishra AK, Ohtsubo M, Li L, Higashi T (2011) Controlling factors of the swelling of various bentonites and their correlations with the hydraulic conductivity of soil-bentonite mixtures. *Appl Clay Sci* 52:78–84
- Sheng DS, Fredlund DGFG, Gens AG (2008) A new modelling approach for unsaturated soils using independent stress. *Can Geotech J* 45:511–534
- Shirazi SM (2010) The influence of temperature on swelling characteristics of compacted bentonite for waste disposal. *Environmentasia* 3:284–286
- Song Y, Davy CA, Troadec D, Blanchenet AM, Skoczylas F, Talandier J, Robinet JC (2015) Multi-scale pore structure of COx claystone: towards the prediction of fluid transport. *Marine Pet Geol* 65:63–82
- Tada S, Watanabe K (2005) Dynamic determination of sorption isotherm of cement based materials. *Cem Concr Res* 35:2271–2277
- Villar MV, Lloret A (2007) Dismantling of the first section of the FEBEX in situ test: THM laboratory tests on the bentonite blocks retrieved. *Phys Chem Earth* 32:716–729
- Villar MV, Lloret A (2008) Influence of dry density and water content on the swelling of a compacted bentonite. *Appl Clay Sci* 39:38–49
- Wang Q, Tang AM, Cui YJ, Delage P, Gatmiri B (2012) Experimental study on the swelling behaviour of bentonite/claystone mixture. *Eng Geol* 124:59–66
- Wang Q, Cui YJ, Tang AM, Barnichon JD, Saba S, Ye WM (2013) Hydraulic conductivity and microstructure changes of compacted bentonite/sand mixture during hydration. *Eng Geol* 164:67–76
- Ye WM, Wan M, Chen B, Chen YG, Cui YJ, Wang J (2013) Temperature effects on the swelling pressure and saturated hydraulic conductivity of the compacted GMZ01 bentonite. *Environ Earth Sci* 68:281–288
- Ye WM, Borrell NC, Zhu JY, Chen B, Chen YG (2014a) Advances on the investigation of the hydraulic behavior of compacted GMZ bentonite. *Eng Geol* 169:41–49
- Ye WM, Zheng ZJ, Chen B, Chen YG, Cui YJ, Wang J (2014b) Effects of pH and temperature on the swelling pressure and hydraulic conductivity of compacted GMZ01 bentonite. *Appl Clay Sci* 101:192–198
- Yen JC, Chang FJ, Chang S (1995) A new criterion for automatic multilevel thresholding. *IEEE Trans Image Process* 4:370–378